THE JOURNAL OF PHYSICAL CHEMISTRY Letters

Letter

Cite This: J. Phys. Chem. Lett. 2019, 10, 5000−5007

pubs.acs.org/JPCL

Lattice Expansion in Hybrid Perovskites: Effect on Optoelectronic Properties and Charge Carrier Dynamics

Dibyajyoti Ghosh,[*,†,‡] Debdipto Acharya,[§] Liujiang Zhou,[∥,†] Wanyi Nie,[⊥] Oleg V. Prezhdo,[#] Sergei Tretiak,[†,‡,@] and Amanda J. Neukirch[*,†]

[†]Theoretical Division, Los Alamos National Laboratory, Los Alamos, New Mexico 87545, United States

[‡]Center for Nonlinear Studies, Los Alamos National Laboratory, Los Alamos, New Mexico 87545, United States

[§]Theoretical Sciences Unit, Jawaharlal Nehru Centre for Advanced Scientific Research, Jakkur, Bangalore 560064, India

[∥]Institute of Fundamental and Frontier Sciences, University of Electronic Science and Technology of China, Chengdu 610054, P. R. China

[⊥]Materials Physics and Applications Division, Los Alamos National Laboratory, Los Alamos, New Mexico 87545, United States

[#]Department of Chemistry, University of Southern California, Los Angeles, California 90089, United States

[@]Center for Integrated Nanotechnologies, Los Alamos National Laboratory, Los Alamos, New Mexico 87545, United States

Supporting Information

ABSTRACT: Hybrid halide perovskites frequently undergo structural expansion due to various stimuli, significantly affecting their electronic properties and in particular their charge carrier dynamics. It is essential to atomistically model how geometric changes modify electronic characteristics that are important for applications such as light harvesting and lighting. Using *ab initio* simulations, here we investigate the structural dynamics and optoelectronic properties of $FAPbI_3$ under tensile strain. The applied strain leads to elongation of the Pb−I bonds and a decrease in the level of PbI_6 octahedral tilting, which manifests as blue-shifts in band gaps. Nonadiabatic molecular dynamics simulations further reveal that charge carrier recombination rates moderately decrease in these expanded lattices. The complex influence of lattice dynamics on electron−phonon scattering results in a longer carrier lifetime, which is advantageous for efficient solar cells. By providing detailed information about the structure−property relationships, this work emphasizes the role of controlled lattice expansion in enhancing the electronic functionalities of hybrid perovskites.

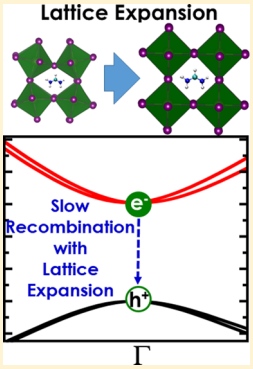

Organic−inorganic hybrid perovskites have emerged as one of the most promising candidates for new-generation light harvesters in photovoltaic devices, photodetectors, and light-emitting diodes.[1−8] The coalescence of many desirable properties such as a long carrier diffusion length, strong visible light absorption, a widely tunable optical band gap, and insensitivity to defects has made halide perovskites highly suitable for many optoelectronic technologies.[9−11] Most studied three-dimensional hybrid lead iodide perovskites have an $APbI_3$ structure, where corner-sharing PbI_6 octahedra form a cuboctahedral cage in which the monovalent organic A cation [e.g., methylammonium $CH_3NH_3^+$ (MA^+) or formamidinium $CH(NH_2)_2^+$ (FA^+)] resides. Due to the mechanical softness of hybrid perovskites, external influences and elemental/molecular size mismatch during compositional engineering give rise to structural distortions.[12−17] The latter considerably influences the long-term stability and performance of perovskite-based devices. Consequently, controlled lattice distortion has been demonstrated as a powerful tool for tuning and optimizing the optoelectronic properties of halide perovskites.[16,18−20] In this regard, improved performances have been reported recently for expanded lattices of these materials.[19−23] Approaches such as mixing large A cations or continuous light illumination of crystals have been applied to precisely control the lattice expansion. As a result, the emerging improved crystallinity, better band alignment with charge-collecting layers, suppressed nonradiative recombination, and longer carrier diffusion all cumulatively boost the photovoltaic efficiencies of these materials. It should also be noted that hybrid perovskite thin films remain under residual strain, which originates from the compositional inhomogeneity and polycrystallinity of the samples.[24−27] Combining several diffraction and microscopy techniques, recent studies have identified the presence of significant tensile strain in mixed (MA/FA) and single (MA) cation perovskites films.[26] This intrinsic residual strain has been suggested to be the reason for largely heterogeneous photoluminescence and restricted charge dynamics in thin films.[28−31] Despite those developments, the effect of tensile strain on the optoelectronic functionalities of halide perovskites has yet to be explored and understood at an atomistic level.

Received: July 12, 2019
Accepted: August 13, 2019
Published: August 13, 2019

DOI: 10.1021/acs.jpclett.9b02020
J. Phys. Chem. Lett. 2019, 10, 5000−5007

In recent studies, we have explored the polaron formation, structural dimensionality reduction, and compositional engineering of halide perovskites.[14,32−38] In the work presented here, we use *ab initio* simulations to investigate the structural evolution of $FAPbI_3$ under tensile strain and its influence on the optoelectronic properties and charge carrier dynamics. We demonstrate that lattice expansion elongates the Pb−I bonds and decreases the level of PbI_6 tilting. These structural changes increase the band gap by decreasing the energy of the valence band edge. This calls for the use of hole-collecting layers with proper energetic band alignment to improve interfacial charge transport. Lattice dynamics exhibit enhanced structural fluctuations in these expanded lattices. Nonadiabatic molecular dynamics (NAMD) simulations further demonstrate that the electron−hole recombination time increases for $FAPbI_3$ under tensile strain. A combination of several factors such as a reduced level of nonadiabatic electron−phonon coupling, quicker decoherence between the participating states, and a blue-shifted band gap results in a slightly longer carrier lifetime, which is beneficial for optoelectronics. Our study concludes that controlled lattice expansion of halide perovskites is a promising route for enhancing device performances.

We start our simulations by investigating the structural response of $FAPbI_3$ under mechanical tensile strain. Initially, two structural models that correspond to the tetragonally distorted low-symmetry orthorhombic phase and the high-symmetry cubic phase were considered. These two structures notably differ by the extent of PbI_6 octahedral tilting (see Figure S1a,b). Optimizing both structures at 0 K, without any constraints or applied tensile strain, we find that the orthorhombic crystal is more stable than the cubic one (Figure S1c). Moreover, to include the finite temperature effects, we performed *ab initio* molecular dynamics (AIMD) simulations on orthorhombic $FAPbI_3$ at 300 K. As shown in Figure S2a, the time-averaged structure is relatively more symmetric with less tilted PbI_6 octahedra. Nevertheless, we find significant symmetry lowering octahedral tilting in the lattice across the instantaneous geometries (Figure S2b). These differences in time-averaged and instantaneous structures agree well with previous experimental and computational studies.[39−41] X-ray diffraction (XRD)-based measurements that provide time-averaged structures with long coherence lengths reported a high-symmetry cubic phase of $FAPbI_3$ at room temperature.[42] However, high isotropic atomic displacement parameters obtained from a neutron diffraction study indicate the presence of considerable octahedral tilting and local distortion in this halide perovskite.[43]

Under lattice expansion, the relative energy difference between the orthorhombic and cubic phases remains almost unchanged (Figure S3), suggesting the former as the ground state phase. Note that recent studies have reported the appearance of a cubic phase with lattice expansion;[20,22] however, our results demonstrate that the local geometry remains distorted with low symmetry under tensile strain. Thus, we investigate the effect of lattice expansion only in the orthorhombic phase.

As shown in Figure 1a and Figure S4a, under isotropic tensile strain, the volume of $FAPbI_3$ increases, expanding all of the lattice parameters. The relative volume expansion in our computational model is within the range reported for the experimental studies based on dimethylammonium (DMA) and guanidinium (GA) mixed perovskites, $MA_{1-x}DMA_xPbI_3$ and $MA_{1-x}GA_xPbI_3$ ($x \leq 0.25$) (see Figure S5).[21,22] The Pb−I

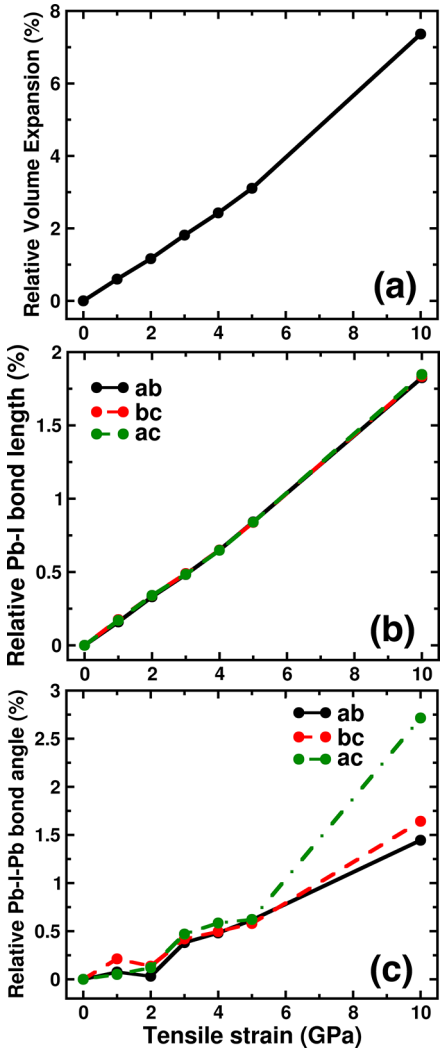

Figure 1. Effect of lattice expansion on the structure of $FAPbI_3$. Relative changes in (a) lattice volume, (b) averaged Pb−I bond length, and (c) Pb−I−Pb angle averaged over three Cartesian planes. The corresponding absolute values are shown in panels a−c of Figure S4, respectively.

bond lengths increase in all spatial directions relatively equally, revealing the isotropic nature of the cell expansion (Figure 1b and Figure S4b). Note that a slightly longer Pb−I bond [0.01 Å (Figure S4b)] along the $a-b$ plane indicates a small tetragonal distortion in the lattice. In addition, as shown in Figure 1c and Figure S4c, the average Pb−I−Pb bond angles along all crystal planes increase with lattice expansion, demonstrating a reduced level of PbI_6 octahedral tilting. Thus, an isotropic tensile strain pushes the entire lattice toward a more symmetric phase as also found in experiment.[19,20,22] However, unlike experimental reports, we did not find any phase transition within the range of applied strain. As mentioned above, this disagreement can arise from the fact that XRD-based experiments poorly capture short time-scale local geometric distortions. Thus, the reported experimental high-symmetry phase can always have a locally distorted low-symmetry structure that our computational study finds as the ground state geometry.

We next explore the effect of tensile strain on the optoelectronic properties of $FAPbI_3$. It is well established that even though semilocal exchange-correlation functionals

DOI: 10.1021/acs.jpclett.9b02020
J. Phys. Chem. Lett. 2019, 10, 5000−5007

can accurately predict the ground state structures of these materials, calculated electronic properties using this level of theory deviate significantly from experimental reports.[11,44] Thus, to correctly simulate the band gap and band edge energies, we include both spin−orbit coupling (SOC) and range-separated hybrid exchange-correlation functionals (HSE06 with a tuned α parameter) in our simulations (see Methods). The band gap, as shown in Figure 2a, shifts to larger

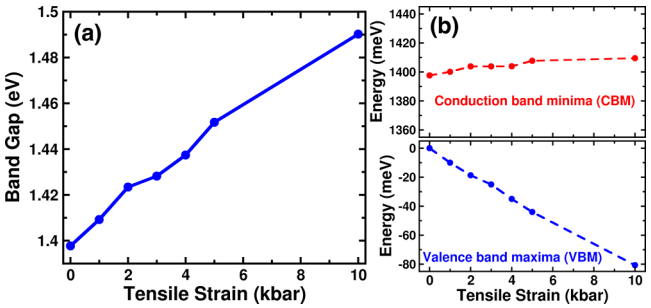

Figure 2. Modification of the electronic properties of $FAPbI_3$ under tensile strain calculated using the HSE06+SOC approach. (a) Blue-shift of the band gap. (b) Energy shift for conduction band minima (CBM, top) and valence band maxima (VBM, bottom). Plotted energies are scaled to the VBM of pristine $FAPbI_3$.

values with enhanced lattice strain, suggesting a blue-shift in the optical absorption spectra. In addition, plotted band structures in Figure S6 exhibit the direct band gap nature of $FAPbI_3$ at the Γ point with or without lattice expansion. This tensile strain-induced band gap increase is quite consistent with the experimental reports in which the lattice expands due to incorporation of large A cations such as GA, DMA, and ethylammonium (EA) ions.[20−23] Note that the effect of strain on the band gap is much smaller than the other tuning approaches such as halide substitution or B metal alloying that change the gap by hundreds to thousands of millielectronvolts.[33,45−47] This suggests lattice strain is a promising tool for fine-tuning the band gap that is strongly desired for hybrid perovskite-based tandem solar cells.[48−50]

The energetic alignments between the frontier bands of halide perovskites and charge transport layers are very crucial for device performance.[51−53] Recently, several studies have indicated that the band alignment is very sensitive to the residual strain present in the perovskite absorber layer.[17,19,26] To model variations in the band edge energies of $FAPbI_3$ under different tensile strains, we aligned all of the bands with respect to a deep state level (see section S1 of the Supporting Information for details).[14,54,55] As shown in Figure 2b (bottom panel), the band edges are sensitive to applied tensile strain. In particular, the energy of the VBM continuously decreases, whereas that of the CBM remains almost unaffected with a slight upshift in response to increased lattice strain. These computational results are in excellent agreement with a recent experimental study based on the combined techniques of electrochemical impedance spectroscopy and transient photovoltage decay measurements.[26] Note that, as discussed in a recent study, the relative band edge positions of low-dimensional halide perovskites can be modified differently under applied strain.[56]

To understand the atomistic reasons for these modified optoelectronic properties, we scrutinized the changes in the electronic nature of $FAPbI_3$ band edges under lattice expansion. The antibonding overlap between Pb (6s) and I (5p) orbitals forms the VB, whereas Pb 6p orbitals predominantly form the CB with a small contribution from I (5p), making the band a largely nonbonded state (see Figure S7 for electronic charge density plots of the VBM and CBM). We further analyzed the crystal orbital Hamilton population (COHP) of these band edges to assess the influence of lattice expansion on these states. The COHP calculates partitioned orbital-pair interactions, that is, the bond-weighted density of states between a pair of neighboring atoms, and its integrated value (ICOHP) provides the bond strength.[57,58] The details of this population analysis can be found in section S2. As shown in Figure 3a, a negative ICOHP value for the valence band, including the Pb 6s and I 5p orbitals, indicates its antibonding character as also found from charge density analysis (Figure S7). Moreover, the ICOHP value for the VB decreases with tensile strain. In contrast, the ICOHP values for the conduction band are much smaller, reconfirming its non-bonding character (see section S2 and Figure S8). As the PbI cages expand through elongation of the Pb−I bonds, the antibonding overlap between Pb 6s and I 5p orbitals in the VB decreases. The reduced level of antibonding in the VBM further shifts its energy level downward as shown in Figure 2b (bottom panel). However, due to its dominant nonbonding orbital overlap, the CB does not change significantly under lattice expansion. Because the CBM level is mostly unchanged, the band gap increases with lattice expansion. Notably, the octahedral tilting of PbI_6 decreases with lattice expansion. This results in more linear Pb−I−Pb angles (Figure 1c), which enhances the antibonding overlap in the VBM. However, changes in the Pb−I bond distances dominate versus changes

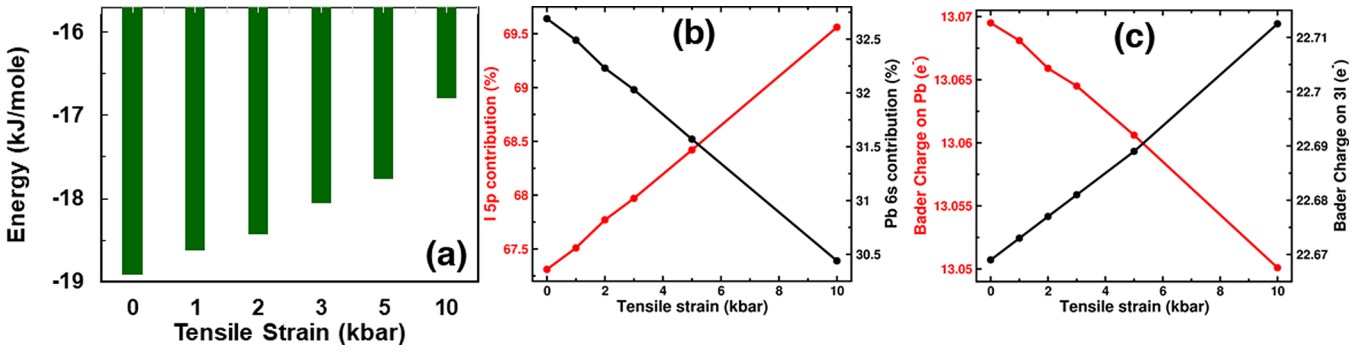

Figure 3. Effect of tensile strain on the band edges and charge distribution in $FAPbI_3$. (a) Integrated COHPs depicting the antibonding strength at the VBM. (b) Relative contribution of I 5p and Pb 6s orbitals to the VBM. (c) Bader charges on Pb and I atoms per formula unit of $FAPbI_3$.

DOI: 10.1021/acs.jpclett.9b02020
J. Phys. Chem. Lett. 2019, 10, 5000−5007

in the Pb−I−Pb angles in influencing the orbital overlap and relative energy position of the VBM.

We additionally analyzed the change in relative orbital contributions to the band edges with lattice expansion. As plotted in Figure 3b, the I (5p) increases whereas Pb (6s) decreases their contribution to VBM. This consequently indicates an enhanced ionic character of this state with a localized charge density on iodide atoms. The contributions of Pb (6p) orbitals to the CBM increase with lattice expansion, although to a lesser extent compared to the respective effect in the VBM (see Figure S9). The calculated atomic Bader charges as plotted in Figure 3c further demonstrate that with lattice expansion, more electrons accumulate on iodide atoms and the lead atoms become more positively charged. This trend in charge redistribution confirms the enhanced ionicity of the Pb−I framework of $FAPbI_3$ subject to tensile strain.

Thus, lattice expansion in $FAPbI_3$ tends to localize the VBM charge density over iodide anions, making the inorganic framework chemically more ionic. However, the CBM remains essentially unaffected by the tensile strain.

The low bulk modulus of the hybrid perovskite lattice gives rise to structural fluctuations even under ambient conditions.[32,59,60] Recent studies demonstrate that such fluctuations significantly influence the photogenerated charge carrier dynamics in these materials.[60−64] We therefore explore the changes in structural motions upon lattice expansion and the effect on carrier dynamics in $FAPbI_3$ by using AIMD (see Methods). Note that, due to large structural fluctuations at high tensile strains, we restrict the MD simulations of $FAPbI_3$ to run under 5 kbar expansive pressure.

In particular, we focus on the dynamics of the PbI framework as it is dominant in accommodating the charge carriers in halide perovskites (see Figure S7). The calculated root-mean-square fluctuations (RMSFs) for Pb and I atoms of $FAPbI_3$ under different tensile strain are shown in Figure 4a.

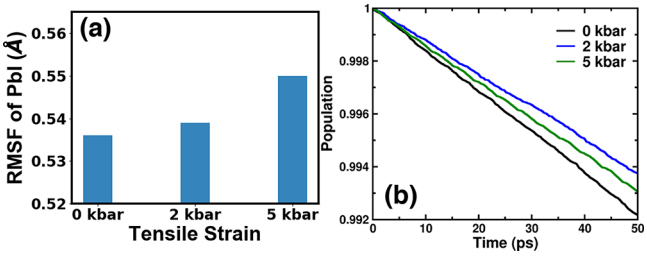

Figure 4. (a) Effect of lattice expansion on lattice dynamics. The root-mean-square fluctuation for PbI at 300 K shows more dynamical behavior under tensile strain. (b) Charge carrier recombination in $FAPbI_3$ under tensile strain. Partial suppression of nonradiative recombination of photogenerated electrons and holes in an expanded lattice.

With the lattice expansion, the RMSFs imply that the number of spatial fluctuations of the PbI frame increases. As the lattice volume increases, the PbI_6 octahedron accesses more space to mutually distort the cage geometry, resulting in a more rotationally disordered structure.

NAMD-based simulations have been performed to link the effect of lattice expansion to the charge carrier dynamics in $FAPbI_3$. To determine the effect of the tensile strain on the nonradiative electron−hole recombination rate, we compute the time-dependent population of the first excited state that has been modeled by exciting an electron from the VBM to the CBM at the Γ point. As shown in Figure 4b, the excited state population decays at a moderately slower rate for the expanded lattice, depicting suppression of charge recombination and a longer carrier lifetime to some extent. The charge recombination time as included in Table 1 is evaluated by using the short time linear approximation of the exponential decay (see the Supporting Information for detail calculations). We find an electron−hole recombination time of 6.3 ns for pristine $FAPbI_3$. The nanosecond time scale for charge recombination is consistent with previous simulations and experimental studies exploring very similar hybrid perovskites.[65−67] Under a tensile strain of 2 kbar, the $FAPbI_3$ lattice decreases the nonradiative decay rate and increases the recombination time to 8.1 ns, which is a relative enhancement of 33%. However, under further lattice expansion (i.e., 5 kbar), the recombination time has been calculated to be 7.2 ns, indicating a slightly increased recombination rate with respect to a smaller tensile strain.

Table 1. Average Absolute Values of Nonadiabatic Coupling, Pure Dephasing Times, and Nonradiative Carrier Recombination Times in $FAPbI_3$ under Different Tensile Strains

tensile strain (kbar)	dephasing time (fs)	NA coupling (meV)	recombination time (ns)
0	3.92	1.8	6.3
2	3.88	1.4	8.1
5	4.12	2.0	7.2

The atomistic reason for the longer carrier recombination time can be understood by analyzing the influence of lattice expansion in terms of several factors such as the dephasing time, nonadiabatic electron−phonon coupling, and band gap fluctuation over time. The recombination rate varies inversely with the band gap and scales as the square of the nonadiabatic coupling strength according to Fermi's golden rule.[68,69] Larger structural and band gap fluctuations along the trajectory indicate enhanced electron−phonon nonadiabatic coupling due to the increased chances of VBM−CBM wave function mixing (see section S3). The dephasing time further influences the recombination rate by being added through the Franck−Condon factor. Physically, during nonradiative charge recombination, a pair of participating states form a coherence between them. Thus, quicker decoherence and weaker nonadiabatic coupling result in a longer recombination time.[69] As shown in Table 1, both nonadiabatic coupling and the dephasing time moderately decrease with the application of a 2 kbar tensile strain in the $FAPbI_3$ lattice. The localization of the VB (Figure 3) and the slight reduction in band gap fluctuation (Table S1) result in a weaker nonadiabatic coupling. These changes, along with a small increase in the average band gap (Table S1), collectively enhance the carrier lifetime of this halide perovskite under tensile strain as shown in Figure 4b. An increase in recombination time with lattice expansion agrees well with the several experimental reports.[21,23] Note that with further increased tensile strain (i.e., 5 kbar) the recombination time decreases due to stronger nonadiabatic coupling and a longer decoherence time. An increase in structural dynamics (Figure 4a) and the number of band gap fluctuations (Table S1) enhance the nonadiabatic coupling, causing accelerated electron−hole recombination. However, a blue-shift in the band gap in this expanded lattice

DOI: 10.1021/acs.jpclett.9b02020
J. Phys. Chem. Lett. 2019, 10, 5000−5007

partially suppresses the recombination, giving rise to a recombination time that is longer than that of the parent $FAPbI_3$. Details of the effects of tensile strain on electron−phonon coupling in $FAPbI_3$ are discussed in the section S3.

In conclusion, our study elucidates the effect of lattice expansion on the structural and optoelectronic properties of $FAPbI_3$. Under tensile strain, the PbI framework is distorted with longer Pb−I bonds and less tilted PbI_6 octahedra. In the expanded lattice, the band gap increases and the valence band maxima decrease, influencing the charge carrier generation and their collection in the interface via modification of interfacial energies. By performing nonradiative charge carrier dynamics, we find that tensile strain slightly decreases the electron−hole recombination rate, indicating probable beneficial effects of lattice expansion on charge carrier dynamics in $FAPbI_3$. Our study suggests that one may fine-tune the lattice expansion to optimize the photovoltaics in these materials. Such precise control over lattice expansion can be achieved by compositional engineering where large A cations (GA and DMA) can partially substitute for FA in $FAPbI_3$. An alternative but more challenging approach can be fine-tuning the growth process during fabrication to incorporate residual tensile strain in the polycrystalline $FAPbI_3$ thin films. By demonstrating the complex relationship between lattice distortion and charge carrier dynamics in halide perovskites, our work provides guidelines for experimental studies to use tensile strain to control electronic functionalities and improve the performance of materials for photovoltaic applications.

METHODS

Density functional theory (DFT)-based simulations, as implemented in the Vienna Ab Initio Simulation Package (VASP), were performed for geometry relaxation and electronic structure calculations.[70,71] The projected augmented-wave (PAW) method using a plane-wave basis set with an energy cut off of 520 eV was applied for all of the calculations.[72] The exchange and correlation interactions were modeled using the generalized gradient approximation (GGA) with the Perdew−Burke−Ernzerhof (PBE) functional form.[73] During geometry optimization of a 2 × 2 × 2 (eight FA cations) supercell, all interatomic forces were relaxed to <0.01 eV $Å^{-1}$, where a 4 × 4 × 4 Γ-centered Monkhorst−Pack[74] mesh was employed. Note that, as various studies have reported dynamic cation−PbI vibrational coupling in hybrid halide perovskites,[60,75] we have applied the DFT-D3 method as suggested by Grimme[76] for all of our static and AIMD simulations. To simulate structural changes with tensile strain, the supercell was reoptimized under static expansive pressures up to a maximum 10 kbar. This range of tensile strains properly models the lattice expansion of the perovskite lattice as reported in several experimental studies (see the Supporting Information for details).[19−23] For the electronic structures, the Brillouin zone integrations were performed in a Γ-centered 6 × 6 × 6 *k*-point mesh with Gaussian smearing of 0.01 eV. Spin−orbit coupling (SOC) and the Heyd−Scuseria−Ernzerhof screened hybrid functionals (HSE06) were further applied self-consistently to correct the electronic structure.[77] Hartree−Fock exchange of 43% was considered for the HSE06 functionals along with an empirical range separation parameter ω of 0.11 b^{-1}. Previous studies have shown that these computational parameters successfully model the near band edge electronic structure of hybrid halide perovskites.[11]

To explore the charge carrier dynamics, the mixed quantum classical NAMD simulations were performed by employing the decoherence-induced surface hopping (DISH) technique.[78,79] In this approach, the lighter electrons and heavier nuclei are treated as quantum mechanical and semiclassical objects, respectively. This method has been widely applied to simulate the excited state dynamics in inorganic and hybrid perovskites.[80−83] *Ab initio* molecular dynamics simulations were performed with a plane-wave energy cutoff of 400 eV, a 3 × 3 × 3 Monkhorst−Pack *k*-point mesh, and a time step of 1 fs. The optimized structures under different tensile strains were heated to 300 K using repeated velocity rescaling for 4 ps. Following that, MD trajectories were simulated for an additional 4 ps in the microcanonical ensemble and considered further for the nonadiabatic coupling calculations. All of the 4000 geometries in the trajectories and 1000 stochastic realizations of the DISH process for each geometry were considered for computing electron−hole recombination using the PYXAID code.[84,85] The pure dephasing time as formulated in the optical-response theory was considered for calculation of the decoherence time.[86] More details about these methods can be found in section S3.

ASSOCIATED CONTENT

Supporting Information

The Supporting Information is available free of charge on the ACS Publications website at DOI: 10.1021/acs.jpclett.9b02020.

Details of the $FAPbI_3$ structure in different phases, phase stability and change in structure under tensile strain, band alignment method, crystal orbital Hamilton population method, and details of charge carrier dynamics in $FAPbI_3$ under tensile strain (PDF)

AUTHOR INFORMATION

Corresponding Authors

*E-mail: dibyajyoti@lanl.gov.
*E-mail: ajneukirch@lanl.gov.

ORCID

Dibyajyoti Ghosh: 0000-0002-3640-7537
Liujiang Zhou: 0000-0001-5814-4486
Oleg V. Prezhdo: 0000-0002-5140-7500
Sergei Tretiak: 0000-0001-5547-3647
Amanda J. Neukirch: 0000-0002-6583-0086

Notes

The authors declare no competing financial interest.

ACKNOWLEDGMENTS

The work at Los Alamos National Laboratory (LANL) was supported by the LANL Laboratory Directed Research and Development Funds (LDRD) program. This work was done in part at the Center for Nonlinear Studies (CNLS) and the Center for Integrated Nanotechnologies (CINT), a U.S. Department of Energy and Office of Basic Energy Sciences user facility, at LANL. This research used resources provided by the LANL Institutional Computing Program. Los Alamos National Laboratory is operated by Triad National Security, LLC, for the National Nuclear Security Administration of the U.S. Department of Energy (Contract 89233218NCA000001). D.A. acknowledges the computing facility provided by TUE-

DOI: 10.1021/acs.jpclett.9b02020
J. Phys. Chem. Lett. 2019, 10, 5000−5007

CMS, JNCASR, India. O.V.P. acknowledges funding from the U.S. Department of Energy via Grant DE-SC0014429.

REFERENCES

(1) Kojima, A.; Teshima, K.; Shirai, Y.; Miyasaka, T. Organometal Halide Perovskites as Visible-light Sensitizers for Photovoltaic Cells. *J. Am. Chem. Soc.* **2009**, *131*, 6050−6051.
(2) Lee, M. M.; Teuscher, J.; Miyasaka, T.; Murakami, T. N.; Snaith, H. J. Efficient Hybrid Solar Cells Based on Meso-superstructured Organometal Halide Perovskites. *Science* **2012**, *338*, 643−647.
(3) Green, M. A.; Ho-Baillie, A.; Snaith, H. J. The Emergence of Perovskite Solar Cells. *Nat. Photonics* **2014**, *8*, 506−514.
(4) Grätzel, M. The Light and Shade of Perovskite Solar Cells. *Nat. Mater.* **2014**, *13*, 838−842.
(5) Dou, L.; Yang, Y. M.; You, J.; Hong, Z.; Chang, W.-H.; Li, G.; Yang, Y. Solution-processed hybrid perovskite photodetectors with high detectivity. *Nat. Commun.* **2014**, *5*, 5404.
(6) Fang, Y.; Dong, Q.; Shao, Y.; Yuan, Y.; Huang, J. Highly narrowband perovskite single-crystal photodetectors enabled by surface-charge recombination. *Nat. Photonics* **2015**, *9*, 679.
(7) Tan, Z.-K.; Moghaddam, R. S.; Lai, M. L.; Docampo, P.; Higler, R.; Deschler, F.; Price, M.; Sadhanala, A.; Pazos, L. M.; Credgington, D.; et al. Bright light-emitting diodes based on organometal halide perovskite. *Nat. Nanotechnol.* **2014**, *9*, 687.
(8) Yuan, M.; Quan, L. N.; Comin, R.; Walters, G.; Sabatini, R.; Voznyy, O.; Hoogland, S.; Zhao, Y.; Beauregard, E. M.; Kanjanaboos, P.; et al. Perovskite energy funnels for efficient light-emitting diodes. *Nat. Nanotechnol.* **2016**, *11*, 872.
(9) Stranks, S. D.; Eperon, G. E.; Grancini, G.; Menelaou, C.; Alcocer, M. J.; Leijtens, T.; Herz, L. M.; Petrozza, A.; Snaith, H. J. Electron-hole diffusion lengths exceeding 1 micrometer in an organometal trihalide perovskite absorber. *Science* **2013**, *342*, 341−344.
(10) Protesescu, L.; Yakunin, S.; Bodnarchuk, M. I.; Krieg, F.; Caputo, R.; Hendon, C. H.; Yang, R. X.; Walsh, A.; Kovalenko, M. V. Nanocrystals of cesium lead halide perovskites (CsPbX3, X= Cl, Br, and I): novel optoelectronic materials showing bright emission with wide color gamut. *Nano Lett.* **2015**, *15*, 3692−3696.
(11) Meggiolaro, D.; De Angelis, F. First-Principles Modeling of Defects in Lead Halide Perovskites: Best Practices and Open Issues. *ACS Energy Lett.* **2018**, *3*, 2206−2222.
(12) Saliba, M.; Matsui, T.; Seo, J.-Y.; Domanski, K.; Correa-Baena, J.-P.; Nazeeruddin, M. K.; Zakeeruddin, S. M.; Tress, W.; Abate, A.; Hagfeldt, A.; Gratzel, M. Cesium-containing Triple Cation Perovskite Solar Cells: Improved Stability, Reproducibility and High Efficiency. *Energy Environ. Sci.* **2016**, *9*, 1989−1997.
(13) McMeekin, D. P.; Sadoughi, G.; Rehman, W.; Eperon, G. E.; Saliba, M.; Hörantner, M. T.; Haghighirad, A.; Sakai, N.; Korte, L.; Rech, B.; Johnston, M. B.; Herz, L. M.; Snaith, H. J. A Mixed-cation Lead Mixed-halide Perovskite Absorber for Tandem Solar Cells. *Science* **2016**, *351*, 151−155.
(14) Ghosh, D.; Smith, A. R.; Walker, A. B.; Islam, M. S. Mixed A-Cation Perovskites for Solar Cells: Atomic-Scale Insights Into Structural Distortion, Hydrogen Bonding, and Electronic Properties. *Chem. Mater.* **2018**, *30*, 5194−5204.
(15) Jaffe, A.; Lin, Y.; Karunadasa, H. I. Halide Perovskites Under Pressure: Accessing New Properties Through Lattice Compression. *ACS Energy Lett.* **2017**, *2*, 1549−1555.
(16) Kong, L.; Liu, G.; Gong, J.; Hu, Q.; Schaller, R. D.; Dera, P.; Zhang, D.; Liu, Z.; Yang, W.; Zhu, K.; et al. Simultaneous band-gap narrowing and carrier-lifetime prolongation of organic−inorganic trihalide perovskites. *Proc. Natl. Acad. Sci. U. S. A.* **2016**, *113*, 8910−8915.
(17) Ghosh, D.; Aziz, A.; Dawson, J. A.; Walker, A. B.; Islam, M. S. Putting the Squeeze on Lead Iodide Perovskites: Pressure-Induced Effects to Tune their Structural and Optoelectronic Behaviour. *Chem. Mater.* **2019**, *31*, 4063−4071.
(18) Wang, P.; Guan, J.; Galeschuk, D. T. K.; Yao, Y.; He, C. F.; Jiang, S.; Zhang, S.; Liu, Y.; Jin, M.; Jin, C.; Song, Y. Pressure-Induced Polymorphic, Optical, and Electronic Transitions of Formamidinium Lead Iodide Perovskite. *J. Phys. Chem. Lett.* **2017**, *8*, 2119−2125.
(19) Tsai, H.; Asadpour, R.; Blancon, J.-C.; Stoumpos, C. C.; Durand, O.; Strzalka, J. W.; Chen, B.; Verduzco, R.; Ajayan, P. M.; Tretiak, S.; et al. Light-induced lattice expansion leads to high-efficiency perovskite solar cells. *Science* **2018**, *360*, 67−70.
(20) Kim, H.-S.; Hagfeldt, A. Photoinduced Lattice Symmetry Enhancement in Mixed Hybrid Perovskites and Its Beneficial Effect on the Recombination Behavior. *Adv. Opt. Mater.* **2019**, *7*, 1801512.
(21) Jodlowski, A. D.; Roldán-Carmona, C.; Grancini, G.; Salado, M.; Ralaiarisoa, M.; Ahmad, S.; Koch, N.; Camacho, L.; De Miguel, G.; Nazeeruddin, M. K. Large guanidinium cation mixed with methylammonium in lead iodide perovskites for 19% efficient solar cells. *Nat. Energy.* **2017**, *2*, 972.
(22) Shao, F.; Qin, P.; Wang, D.; Zhang, G.; Wu, B.; He, J.; Peng, W.; Sum, T. C.; Wang, D.; Huang, F. Enhanced Photovoltaic Performance and Thermal Stability of CH3NH3PbI3 Perovskite through Lattice Symmetrization. *ACS Appl. Mater. Interfaces* **2019**, *11*, 740−746.
(23) Gholipour, S.; Ali, A. M.; Correa-Baena, J.-P.; Turren-Cruz, S.-H.; Tajabadi, F.; Tress, W.; Taghavinia, N.; Grätzel, M.; Abate, A.; De Angelis, F.; et al. Globularity-Selected Large Molecules for a New Generation of Multication Perovskites. *Adv. Mater.* **2017**, *29*, 1702005.
(24) Jones, T. W.; Osherov, A.; Alsari, M.; Sponseller, M.; Duck, B. C.; Jung, Y.-K.; Settens, C.; Niroui, F.; Brenes, R.; Stan, C. V.; et al. Local Strain Heterogeneity Influences the Optoelectronic Properties of Halide Perovskites. *Energy Environ. Sci.* **2019**, *12*, 596.
(25) Zhao, J.; Deng, Y.; Wei, H.; Zheng, X.; Yu, Z.; Shao, Y.; Shield, J. E.; Huang, J. Strained hybrid perovskite thin films and their impact on the intrinsic stability of perovskite solar cells. *Sci. Adv.* **2017**, *3*, eaao5616.
(26) Zhu, C.; Niu, X.; Fu, Y.; Li, N.; Hu, C.; Chen, Y.; He, X.; Na, G.; Liu, P.; Zai, H.; et al. Strain engineering in perovskite solar cells and its impacts on carrier dynamics. *Nat. Commun.* **2019**, *10*, 815.
(27) Rolston, N.; Bush, K. A.; Printz, A. D.; Gold-Parker, A.; Ding, Y.; Toney, M. F.; McGehee, M. D.; Dauskardt, R. H. Engineering Stress in Perovskite Solar Cells to Improve Stability. *Adv. Energy Mater.* **2018**, *8*, 1802139.
(28) de Quilettes, D. W.; Vorpahl, S. M.; Stranks, S. D.; Nagaoka, H.; Eperon, G. E.; Ziffer, M. E.; Snaith, H. J.; Ginger, D. S. Impact of microstructure on local carrier lifetime in perovskite solar cells. *Science* **2015**, *348*, 683−686.
(29) Guo, Z.; Manser, J. S.; Wan, Y.; Kamat, P. V.; Huang, L. Spatial and temporal imaging of long-range charge transport in perovskite thin films by ultrafast microscopy. *Nat. Commun.* **2015**, *6*, 7471.
(30) Leblebici, S. Y.; Leppert, L.; Li, Y.; Reyes-Lillo, S. E.; Wickenburg, S.; Wong, E.; Lee, J.; Melli, M.; Ziegler, D.; Angell, D. K.; et al. Facet-dependent photovoltaic efficiency variations in single grains of hybrid halide perovskite. *Nat. Energy* **2016**, *1*, 16093.
(31) deQuilettes, D. W.; Jariwala, S.; Burke, S.; Ziffer, M. E.; Wang, J. T.-W.; Snaith, H. J.; Ginger, D. S. Tracking Photoexcited Carriers in Hybrid Perovskite Semiconductors: Trap-Dominated Spatial Heterogeneity and Diffusion. *ACS Nano* **2017**, *11*, 11488−11496.
(32) Ghosh, D.; Walsh Atkins, P.; Islam, M. S.; Walker, A. B.; Eames, C. Good Vibrations: Locking of Octahedral Tilting in Mixed-Cation Iodide Perovskites for Solar Cells. *ACS Energy Lett.* **2017**, *2*, 2424−2429.
(33) Nagane, S.; Ghosh, D.; Hoye, R. L.; Zhao, B.; Ahmad, S.; Walker, A. B.; Islam, M. S.; Ogale, S.; Sadhanala, A. Lead-Free Perovskite Semiconductors Based on Germanium−Tin Solid Solutions: Structural and Optoelectronic Properties. *J. Phys. Chem. C* **2018**, *122*, 5940−5947.
(34) Neukirch, A. J.; Nie, W.; Blancon, J.-C.; Appavoo, K.; Tsai, H.; Sfeir, M. Y.; Katan, C.; Pedesseau, L.; Even, J.; Crochet, J. J.; et al. Polaron stabilization by cooperative lattice distortion and cation rotations in hybrid perovskite materials. *Nano Lett.* **2016**, *16*, 3809−3816.

DOI: 10.1021/acs.jpclett.9b02020
J. Phys. Chem. Lett. 2019, 10, 5000−5007

(35) Neukirch, A. J.; Abate, I. I.; Zhou, L.; Nie, W.; Tsai, H.; Pedesseau, L.; Even, J.; Crochet, J. J.; Mohite, A. D.; Katan, C.; Tretiak, S. Geometry Distortion and Small Polaron Binding Energy Changes with Ionic Substitution in Halide Perovskites. *J. Phys. Chem. Lett.* **2018**, *9*, 7130−7136.
(36) Park, M.; Neukirch, A. J.; Reyes-Lillo, S. E.; Lai, M.; Ellis, S. R.; Dietze, D.; Neaton, J. B.; Yang, P.; Tretiak, S.; Mathies, R. A. Excited-state vibrational dynamics toward the polaron in methylammonium lead iodide perovskite. *Nat. Commun.* **2018**, *9*, 2525.
(37) Tsai, H.; Nie, W.; Blancon, J.-C.; Stoumpos, C. C.; Asadpour, R.; Harutyunyan, B.; Neukirch, A. J.; Verduzco, R.; Crochet, J. J.; Tretiak, S.; et al. High-efficiency two-dimensional Ruddlesden−Popper perovskite solar cells. *Nature* **2016**, *536*, 312.
(38) Zhou, L.; Katan, C.; Nie, W.; Tsai, H.; Pedesseau, L.; Crochet, J. J.; Even, J.; Mohite, A. D.; Tretiak, S.; Neukirch, A. J. Cation Alloying Delocalizes Polarons in Lead-halide Perovskites. *J. Phys. Chem. Lett.* **2019**, *10*, 3516−3524.
(39) Sutton, R. J.; Filip, M. R.; Haghighirad, A. A.; Sakai, N.; Wenger, B.; Giustino, F.; Snaith, H. J. Cubic or Orthorhombic? Revealing the Crystal Structure of Metastable Black-phase CsPbI3 by Theory and Experiment. *ACS Energy Lett.* **2018**, *3*, 1787−1794.
(40) Worhatch, R. J.; Kim, H.; Swainson, I. P.; Yonkeu, A. L.; Billinge, S. J. Study of Local Structure in Selected Organic−Inorganic Perovskites in the Pm3m Phase. *Chem. Mater.* **2008**, *20*, 1272−1277.
(41) Zhao, X.; Dalpian, G. M.; Wang, Z.; Zunger, A. The polymorphous nature of cubic halide perovskites. *arXiv* **2019**, 1905.09141.
(42) Fabini, D. H.; Stoumpos, C. C.; Laurita, G.; Kaltzoglou, A.; Kontos, A. G.; Falaras, P.; Kanatzidis, M. G.; Seshadri, R. Reentrant Structural and Optical Properties and Large Positive Thermal Expansion in Perovskite Formamidinium Lead Iodide. *Angew. Chem., Int. Ed.* **2016**, *55*, 15392−15396.
(43) Weller, M. T.; Weber, O. J.; Frost, J. M.; Walsh, A. Cubic perovskite structure of black formamidinium lead iodide, α-[HC(NH$_2$)$_2$]PbI$_3$, at 298 K. *J. Phys. Chem. Lett.* **2015**, *6*, 3209−3212.
(44) Even, J.; Pedesseau, L.; Jancu, J.-M.; Katan, C. Importance of spin−orbit coupling in hybrid organic/inorganic perovskites for photovoltaic applications. *J. Phys. Chem. Lett.* **2013**, *4*, 2999−3005.
(45) Akkerman, Q. A.; D'Innocenzo, V.; Accornero, S.; Scarpellini, A.; Petrozza, A.; Prato, M.; Manna, L. Tuning the optical properties of cesium lead halide perovskite nanocrystals by anion exchange reactions. *J. Am. Chem. Soc.* **2015**, *137*, 10276−10281.
(46) Ono, L. K.; Juarez-Perez, E. J.; Qi, Y. Progress on perovskite materials and solar cells with mixed cations and halide anions. *ACS Appl. Mater. Interfaces* **2017**, *9*, 30197−30246.
(47) Hao, F.; Stoumpos, C. C.; Chang, R. P.; Kanatzidis, M. G. Anomalous band gap behavior in mixed Sn and Pb perovskites enables broadening of absorption spectrum in solar cells. *J. Am. Chem. Soc.* **2014**, *136*, 8094−8099.
(48) McMeekin, D. P.; Sadoughi, G.; Rehman, W.; Eperon, G. E.; Saliba, M.; Hörantner, M. T.; Haghighirad, A.; Sakai, N.; Korte, L.; Rech, B.; Johnston, M.; Herz, L.; Snaith, H. A mixed-cation lead mixed-halide perovskite absorber for tandem solar cells. *Science* **2016**, *351*, 151−155.
(49) Eperon, G. E.; Leijtens, T.; Bush, K. A.; Prasanna, R.; Green, T.; Wang, J. T.-W.; McMeekin, D. P.; Volonakis, G.; Milot, R. L.; May, R.; Snaith, H.; et al. Perovskite-perovskite tandem photovoltaics with optimized band gaps. *Science* **2016**, *354*, 861−865.
(50) Palmstrom, A. F.; Eperon, G. E.; Leijtens, T.; Prasanna, R.; Habisreutinger, S. N.; Nemeth, W.; Gaulding, E. A.; Dunfield, S. P.; Reese, M.; Nanayakkara, S. Enabling Flexible All-Perovskite Tandem Solar Cells. *Joule* **2019**, DOI: 10.1016/j.joule.2019.05.009.
(51) Correa Baena, J. P.; Steier, L.; Tress, W.; Saliba, M.; Neutzner, S.; Matsui, T.; Giordano, F.; Jacobsson, T. J.; Kandada, A. R. S.; et al. Highly efficient planar perovskite solar cells through band alignment engineering. *Energy Environ. Sci.* **2015**, *8*, 2928−2934.
(52) Yin, W.-J.; Yang, J.-H.; Kang, J.; Yan, Y.; Wei, S.-H. Halide perovskite materials for solar cells: a theoretical review. *J. Mater. Chem. A* **2015**, *3*, 8926−8942.
(53) Lim, K.-G.; Kim, H.-B.; Jeong, J.; Kim, H.; Kim, J. Y.; Lee, T.-W. Boosting the power conversion efficiency of perovskite solar cells using self-organized polymeric hole extraction layers with high work function. *Adv. Mater.* **2014**, *26*, 6461−6466.
(54) Yi, C.; Luo, J.; Meloni, S.; Boziki, A.; Ashari-Astani, N.; Grätzel, C.; Zakeeruddin, S. M.; Röthlisberger, U.; Grätzel, M. Entropic Stabilization of Mixed A-cation ABX$_3$Metal Halide Perovskites for High Performance Perovskite Solar Cells. *Energy Environ. Sci.* **2016**, *9*, 656−662.
(55) Meloni, S.; Palermo, G.; Ashari-Astani, N.; Grätzel, M.; Rothlisberger, U. Valence and conduction band tuning in halide perovskites for solar cell applications. *J. Mater. Chem. A* **2016**, *4*, 15997−16002.
(56) Kumavat, S. R.; Sonvane, Y.; Singh, D.; Gupta, S. K. Two-Dimensional CH3NH3PbI3 with High Efficiency and Superior Carrier Mobility: A Theoretical Study. *J. Phys. Chem. C* **2019**, *123*, 5231−5239.
(57) Dronskowski, R.; Blöchl, P. E. Crystal orbital Hamilton populations (COHP): energy-resolved visualization of chemical bonding in solids based on density-functional calculations. *J. Phys. Chem.* **1993**, *97*, 8617−8624.
(58) Deringer, V. L.; Tchougréeff, A. L.; Dronskowski, R. Crystal orbital Hamilton population (COHP) analysis as projected from plane-wave basis sets. *J. Phys. Chem. A* **2011**, *115*, 5461−5466.
(59) Mattoni, A.; Filippetti, A.; Caddeo, C. Modeling hybrid perovskites by molecular dynamics. *J. Phys.: Condens. Matter* **2017**, *29*, 043001.
(60) Yaffe, O.; Guo, Y.; Tan, L. Z.; Egger, D. A.; Hull, T.; Stoumpos, C. C.; Zheng, F.; Heinz, T. F.; Kronik, L.; G, K. M.; et al. Local polar fluctuations in lead halide perovskite crystals. *Phys. Rev. Lett.* **2017**, *118*, 136001.
(61) Stroppa, A.; Di Sante, D.; Barone, P.; Bokdam, M.; Kresse, G.; Franchini, C.; Whangbo, M.-H.; Picozzi, S. Tunable ferroelectric polarization and its interplay with spin−orbit coupling in tin iodide perovskites. *Nat. Commun.* **2014**, *5*, 5900.
(62) Niesner, D.; Hauck, M.; Shrestha, S.; Levchuk, I.; Matt, G. J.; Osvet, A.; Batentschuk, M.; Brabec, C.; Weber, H. B.; Fauster, T. Structural fluctuations cause spin-split states in tetragonal (CH 3 NH 3) PbI 3 as evidenced by the circular photogalvanic effect. *Proc. Natl. Acad. Sci. U. S. A.* **2018**, *115*, 9509−9514.
(63) Motta, C.; El-Mellouhi, F.; Kais, S.; Tabet, N.; Alharbi, F.; Sanvito, S. Revealing the role of organic cations in hybrid halide perovskite CH 3 NH 3 PbI 3. *Nat. Commun.* **2015**, *6*, 7026.
(64) Ma, J.; Wang, L.-W. Nanoscale charge localization induced by random orientations of organic molecules in hybrid perovskite CH3NH3PbI3. *Nano Lett.* **2015**, *15*, 248−253.
(65) Li, W.; Sun, Y.-Y.; Li, L.; Zhou, Z.; Tang, J.; Prezhdo, O. V. Control of charge recombination in perovskites by oxidation state of halide vacancy. *J. Am. Chem. Soc.* **2018**, *140*, 15753−15763.
(66) Li, W.; Tang, J.; Casanova, D.; Prezhdo, O. V. Time-domain ab initio analysis rationalizes the unusual temperature dependence of charge carrier relaxation in lead halide perovskite. *ACS Energy Lett.* **2018**, *3*, 2713−2720.
(67) Tong, C.-J.; Li, L.; Liu, L.-M.; Prezhdo, O. V. Long Carrier Lifetimes in PbI2-Rich Perovskites Rationalized by Ab Initio Nonadiabatic Molecular Dynamics. *ACS Energy Lett.* **2018**, *3*, 1868−1874.
(68) Englman, R.; Jortner, J. The energy gap law for non-radiative decay in large molecules. *J. Lumin.* **1970**, *1*, 134−142.
(69) Long, R.; Prezhdo, O. V.; Fang, W. Nonadiabatic charge dynamics in novel solar cell materials. *Wiley Interdiscip. Rev. Comput. Mol.* **2017**, *7*, No. e1305.
(70) Kresse, G.; Hafner, J. Ab initio molecular dynamics for liquid metals. *Phys. Rev. B: Condens. Matter Mater. Phys.* **1993**, *47*, 558.
(71) Kresse, G.; Hafner, J. Ab initio molecular-dynamics simulation of the liquid-metal−amorphous-semiconductor transition in germanium. *Phys. Rev. B: Condens. Matter Mater. Phys.* **1994**, *49*, 14251.

DOI: 10.1021/acs.jpclett.9b02020
J. Phys. Chem. Lett. 2019, 10, 5000−5007

(72) Kresse, G.; Joubert, D. From ultrasoft pseudopotentials to the projector augmented-wave method. *Phys. Rev. B: Condens. Matter Mater. Phys.* **1999**, *59*, 1758.
(73) Perdew, J. P.; Burke, K.; Ernzerhof, M. Generalized Gradient Approximation Made Simple. *Phys. Rev. Lett.* **1996**, *77*, 3865.
(74) Monkhorst, H. J.; Pack, J. D. Special points for Brillouin-zone integrations. *Phys. Rev. B* **1976**, *13*, 5188.
(75) Grechko, M.; Bretschneider, S. A.; Vietze, L.; Kim, H.; Bonn, M. Vibrational coupling between organic and inorganic sublattices of hybrid perovskites. *Angew. Chem., Int. Ed.* **2018**, *57*, 13657−13661.
(76) Grimme, S.; Antony, J.; Ehrlich, S.; Krieg, H. A consistent and accurate ab initio parametrization of density functional dispersion correction (DFT-D) for the 94 elements H-Pu. *J. Chem. Phys.* **2010**, *132*, 154104.
(77) Heyd, J.; Scuseria, G. E.; Ernzerhof, M. Hybrid functionals based on a screened Coulomb potential. *J. Chem. Phys.* **2003**, *118*, 8207−8215.
(78) Jaeger, H. M.; Fischer, S.; Prezhdo, O. V. Decoherence-induced surface hopping. *J. Chem. Phys.* **2012**, *137*, 22A545.
(79) Craig, C. F.; Duncan, W. R.; Prezhdo, O. V. Trajectory surface hopping in the time-dependent Kohn-Sham approach for electron-nuclear dynamics. *Phys. Rev. Lett.* **2005**, *95*, 163001.
(80) Zhang, Z.; Fang, W.-H.; Tokina, M. V.; Long, R.; Prezhdo, O. V. Rapid decoherence suppresses charge recombination in multi-layer 2D halide perovskites: Time-domain ab initio analysis. *Nano Lett.* **2018**, *18*, 2459−2466.
(81) Long, R.; Liu, J.; Prezhdo, O. V. Unravelling the effects of grain boundary and chemical doping on electron−hole recombination in CH3NH3PbI3 perovskite by time-domain atomistic simulation. *J. Am. Chem. Soc.* **2016**, *138*, 3884−3890.
(82) He, J.; Vasenko, A. S.; Long, R.; Prezhdo, O. V. Halide composition controls electron−hole recombination in cesium−lead halide perovskite quantum dots: a time domain ab initio study. *J. Phys. Chem. Lett.* **2018**, *9*, 1872−1879.
(83) Li, W.; Liu, J.; Bai, F.-Q.; Zhang, H.-X.; Prezhdo, O. V. Hole trapping by iodine interstitial defects decreases free carrier losses in perovskite solar cells: a time-domain ab initio study. *ACS Energy Lett.* **2017**, *2*, 1270−1278.
(84) Akimov, A. V.; Prezhdo, O. V. The PYXAID program for non-adiabatic molecular dynamics in condensed matter systems. *J. Chem. Theory Comput.* **2013**, *9*, 4959−4972.
(85) Akimov, A. V.; Prezhdo, O. V. Advanced capabilities of the PYXAID program: integration schemes, decoherence effects, multi-excitonic states, and field-matter interaction. *J. Chem. Theory Comput.* **2014**, *10*, 789−804.
(86) Hamm, P. *Principles of nonlinear optical spectroscopy: A practical approach*; Oxford University Press: New York, 2005; Vol. *41*, p 77.

DOI: 10.1021/acs.jpclett.9b02020
J. Phys. Chem. Lett. 2019, 10, 5000−5007